JAERI-Tech
2002-033

DESIGN OF NEUTRON MONITOR USING FLOWING WATER ACTIVATION FOR ITER

March 2002

Takeo NISHITANI, Katsuyuki EBISAWA, Chris WALKER* and Satoshi KASAI

日本原子力研究所
Japan Atomic Energy Research Institute

本レポートは、日本原子力研究所が不定期に公刊している研究報告書です。
入手の問合わせは、日本原子力研究所研究情報部研究情報課（〒319-1195　茨城県那珂郡東海村）あて、お申し越しください。なお、このほかに財団法人原子力弘済会資料センター（〒319-1195　茨城県那珂郡東海村日本原子力研究所内）で複写による実費頒布をおこなっております。

This report is issued irregularly.
Inquiries about availability of the reports should be addressed to Research Information Division, Department of Intellectual Resources, Japan Atomic Energy Research Institute, Tokai-mura, Naka-gun, Ibaraki-ken 319-1195, Japan.

編集兼発行　日本原子力研究所

JAERI-Tech 2002-033

Design of Neutron Monitor using Flowing Water Activation for ITER

Takeo NISHITANI, Katsuyuki EBISAWA+, Chris WALKER* and Satoshi KASAI

Department of Fusion Engineering Research
(Tokai Site)
Naka Fusion Research Establishment
Japan Atomic Energy Research Institute
Tokai-mura, Naka-gun, Ibaraki-ken

(Received January 30, 2002)

A neutron monitor with flowing water based on the $^{16}O(n,p)^{16}N$ reaction has been designed for ITER. Irradiation ends will be installed in the filler shielding module between the blanket modules at the horizontal ports. The γ-ray counting stations will be installed on the upstairs of the pit. The distance between the irradiation end and the counting station is ~20 m. We evaluated the performance of this fusion monitor by using MCNP-4b code with the JENDL 3.2 library, where the vacuum vessel, blanket modules, filler shielding modules and first walls were modeled 3-dimensionally. The reaction rate of $^{16}O(n,p)^{16}N$ was calculated not only at the irradiation end but also along the transfer line, which showed that the temporal resolution would be less than the ITER requirement of 100 ms including turbulent diffusion effects for the flow velocity of 10 m/s. With a flow velocity of 10 m/s, this system can measure the fusion power from 50 kW to 500 MW of the ITER operation. Also the calculation shows that the reaction rate is relatively insensitive to the change of the plasma position.

Keywords: Neutron Monitor, Activation, 14-MeV Neutrons, Oxygen 16, Nitrogen 16, Flowing Water, ITER, MCNP-4b, JENDL 3.2

This work is conducted as an ITER Engineering Activities as this report corresponds to ITER Design Task Agreement on "Diagnostics Design" (N 55 TD 02.04FJ).

+ Department of ITER Project (Present address: Toshiba Corp.)

* ITER Joint Central Team, Garching

流水の放射化を用いたITER用中性子モニターの設計

日本原子力研究所那珂研究所核融合工学部
西谷　健夫・海老澤　克之+・Chris WALKER*・河西　敏

(2002年1月30日受理)

$^{16}O(n,p)^{16}N$反応に着目し、流水の放射化を利用したITER用中性子モニターの設計を行った。照射端は赤道面のフィラー遮蔽モジュール内に真空容器を貫通して挿入する構造とした。ガンマ線測定ステーションは生体遮蔽外の上部ピットに設置し、照射端からの距離は20mとした。この配置に基づき、真空容器、ブランケットモジュール、フィラー遮蔽モジュール、第1壁を3次元モデルし、JENDL 3.2核データライブラリーを使用したMCNP-4bコードを用いて各種特性を評価した。時間分解能は水配管に沿った放射化反応の分布及び乱流拡散を考慮して、10m/sの流速に対しITER要求値の時間分解能100ms以下で、50kW-500MWのITERの出力範囲で測定が可能であることを示した。また放射化量はプラズマの位置にほとんど依存しないことが分った。

本研究はＩＴＥＲ工学設計活動の一環として実施したもので、本報告は設計タスク協定(N55 TD02.04FJ)に基づくものである。

那珂研究所（東海駐在）：〒319-1195 茨城県那珂郡東海村白方白根2-4
+　ITER開発室（現（株）東芝）
*　ITERガルヒンク共同センター

Contents

目　次

1. INTRODUCTIONS

1.1 Introduction

The neutron activation method using solid metal sample is used for an accurate measurement of the neutron yield in many fusion devices without temporal resolution. We have proposed a neutron activation of flowing water based on the $^{16}O(n,p)^{16}N$ reaction for the accurate fusion power monitor with reasonable temporal resolution for ITER.

When water is irradiated by 14 MeV neutrons, radioactive ^{16}N nuclei are produced by the $^{16}O(n, p)^{16}N$ reactions from oxygen atoms in the water molecules. A ^{16}N nucleus emits 6.13 (68.8%) and 7.12 (4.7%) MeV γ-rays accompanied by disintegration with the half-life of 7.13 seconds[1]. Since the threshold energy for the $^{16}O(n, p)^{16}N$ reaction is located at 10.4 MeV[2], ^{16}N nuclei are practically produced only by 14 MeV neutrons generated by D-T reactions in the fusion reactor. ^{16}N nuclei are mainly produced in water coolant. In ITER, it was suggested that the high-energy γ-ray irradiation on supper conducting magnets and insulators spoiled their capabilities[3]. Consequently, a sufficient protection against the γ-ray irradiation was adopted at a design of ITER-FEAT. On the other hand, positive usage of the reaction, i.e., a fusion power monitor based on activation of water flow for ITER, was proposed first by Sano et al [4] at ITER-CDA. Smith and Ikeda et al. reported experimental studies on the principle feasibility of the fusion power monitor elsewhere[5,6]. In contrast, Barns et al. made estimations on the capability of the fusion power monitor based upon a limited experimental data [7], where they concluded that the fusion power monitor did not have big advantages.

We studied the technical feasibility of the fusion power monitor based on neutron activation of flowing water by using the D-T neutron source at the Fusion Neutronics Source (FNS) facility[8] of Japan Atomic Energy Research Institute as the ITER/EDA R&D Task T499, where the time resolution of 50 ms and the accuracy of < 10% was obtained [9].

Here we carried out the design work on the neutron activation of flowing water for fusion power monitor of ITER-FEAT based on the recent results on the related R&D, "Neutron Activation with fluid flow" (ITER R&D task T499).

1.2 Functions

The most important advantage of the neutron activation system with fluid flow is that fusion power can be measured in an absolute value similar to a neutron activation method with a solid foil. Moreover, this monitor allows continuous measurement of the fusion power with moderate time resolution of typically 100 ms. The monitor is easily maintained, because the measurement station is located outside of the bio-shield, and there is only the water pipe loop inside the bio-shield. In addition, no long-term sensitivity change is expected. This system could not be used for a real time feedback control due to the time delay of ~1 sec.

The function of the neutron activation system with fluid flow is

- to provide a robust absolute measurement of fusion power with moderate time resolution, stability and wide dynamic range, and
- to allow an absolute calibration of the fusion power for neutron flux monitors and other neutron systems.

1.3 Design Requirements

Target measurement requirements for the neutron activation system with fluid flow are listed in Table 1.2-1. The Neutron Activation System supports other systems (WBS 5.5.B.01, 5.5.B.02, 5.5.B.03, and 5.5.B.04) in satisfying these specifications.

Table 1.2-1 Target Measurement Requirements.

Total Neutron Flux

Parameter	Parameter range	Spatial Resolution	Time Resolution	Accuracy
Total neutron flux	10^{16}-10^{21} n s^{-1}	integral	100 ms	10%
Fusion power	< 1GW	integral	100 ms	10%

2. CONCEPT DESIGN DESCRIPTION

2.1 Concept of the Measurement

The neutron activation system with fluid flow [10] consists of a closed water loop laid between the first wall/blanket region and a remote low-background location as shown in Fig.2.1-1. By measuring the γ-rays from ^{16}N with a γ-ray detector placed beside the water loop, we can determine the D-T neutron yield continuously. The activated water will stay in a reservoir tank to diminish the activity and will be transferred to the first wall/blanket region again.

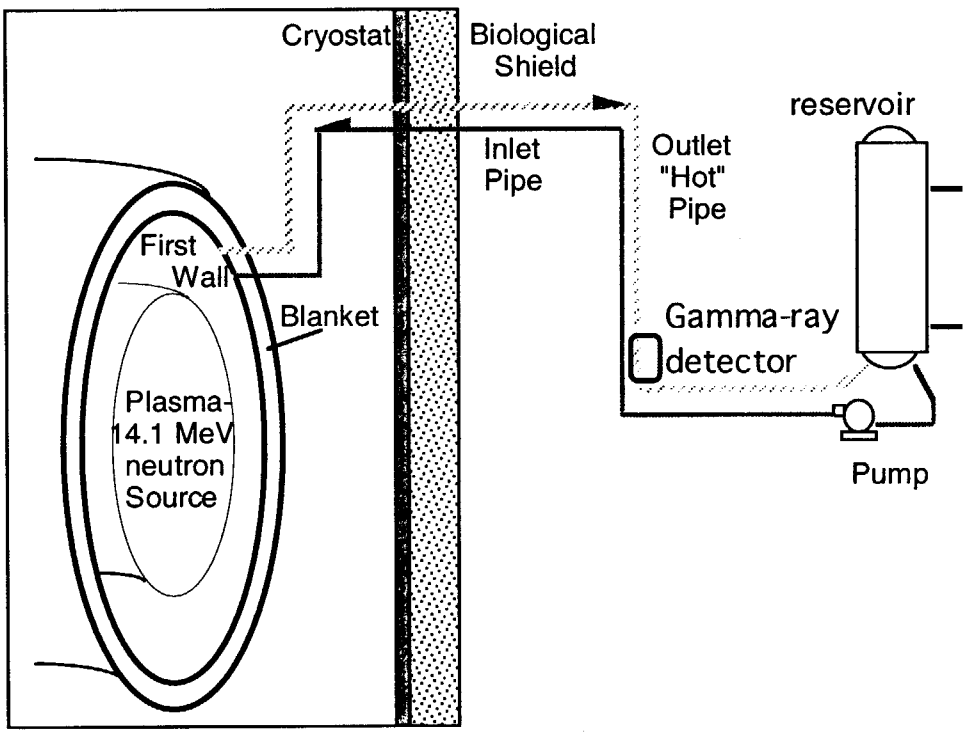

Figure 2.1-1 Concept of neutron activation system with fluid flow.

The cross-section of the $^{16}O(n,p)^{16}N$ reaction is shown in Fig. 2.1-2. The cross-section has a high threshold energy of 10.24 MeV. Therefore, the neutron activation is sensitive for almost virgin neutrons. A ^{16}N nucleus emits 6.13 (68.8%) and 7.12 (4.7%) MeV γ-rays with a half-life of 7.13 seconds.

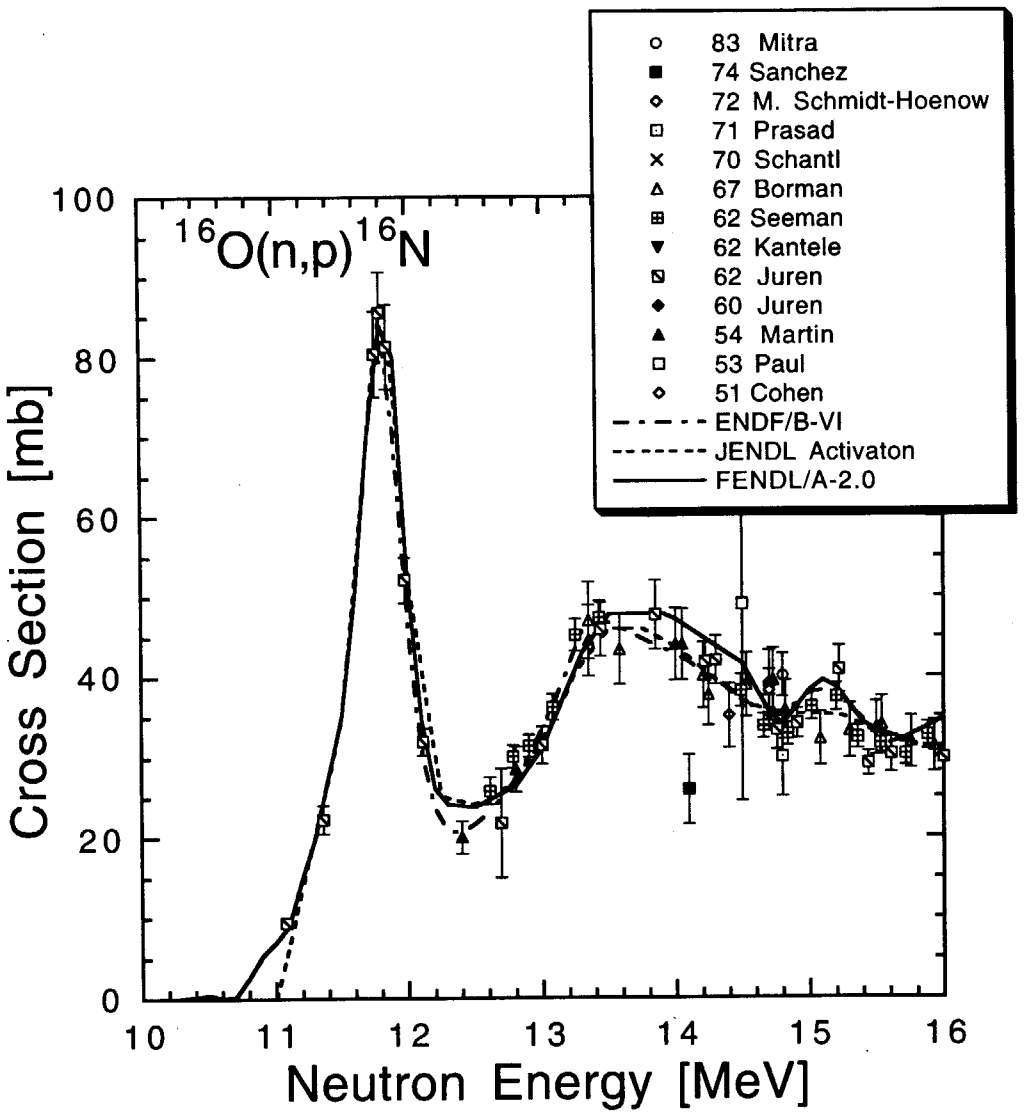

Figure 2.1-2 cross-section of the $^{16}O(n,p)^{16}N$ reaction.

2.2 Basic Theory of the Measurement

The configuration of calculation is shown in Fig.2.2-1. The reaction rate of the $^{16}O(n,p)^{16}N$ reaction in unit mass water in the irradiation region is represented by

$$R = N\int \phi(E)\sigma(E)dE \tag{2.2-1}$$

where N is the atomic density of Oxygen in water, $\sigma(E)$ is the cross section of the $^{16}O(n,p)^{16}N$ reaction, and $\phi(E)$ is the neutron spectrum in the irradiation region. If the neutron spectrum is distributed in the irradiation region, the averaged reaction probability is

$$\bar{R} = \frac{1}{L_0}\int R(L)dL \tag{2.2-2}$$

where L_0 is the length of the irradiation region. The total activity of ^{16}N nuclei in the detectable region of the γ-ray counting station is

$$A = \lambda \bar{R}\frac{L_0}{v}\exp\left(-\lambda\frac{L_1}{v}\right)\left(\rho L_d \pi r^2\right) \tag{2.2-3}$$

where λ is the decay constant of ^{16}N (0.0972 s^{-1}), v is the flow velocity and ρ is the density of water. It is assumed that the residence time in the irradiation region L_0/v is sufficiently shorter than $1/\lambda$. The count rate of the γ-ray detector C is represented by

$$C = \varepsilon A \tag{2.2-4}$$

Where ε is the detection efficiency for unit activity of ^{16}N nuclei, which includes an intrinsic detection efficiency of the detector, a geometrical efficiency, and γ-ray emission probability for unit activity. When the traveling time t is defined by L_1/v,

$$\frac{dC}{dt} \propto (1-\lambda t)\exp(-\lambda t) \tag{2.2-5}$$

The count rate will be maximum at $t=1/\lambda$ (10.288 sec) as shown in Fig.2.2-2.

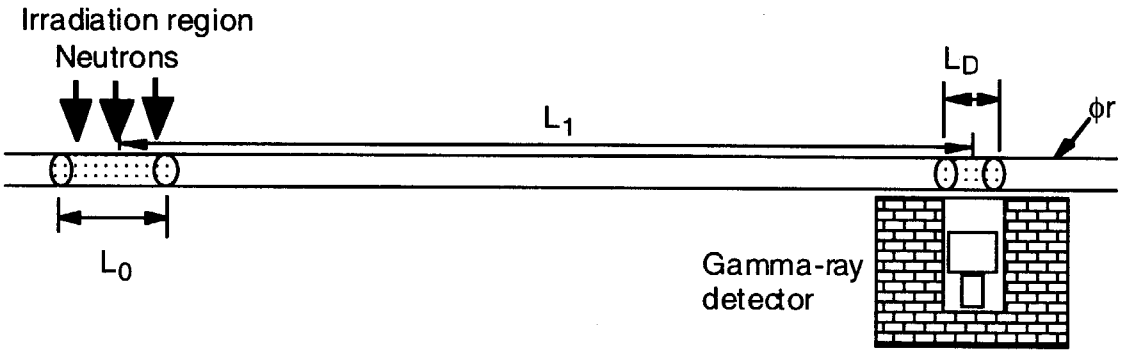

Figure 2.2-1 Configuration of the calculation for the neutron activation measurement with fluid flow.

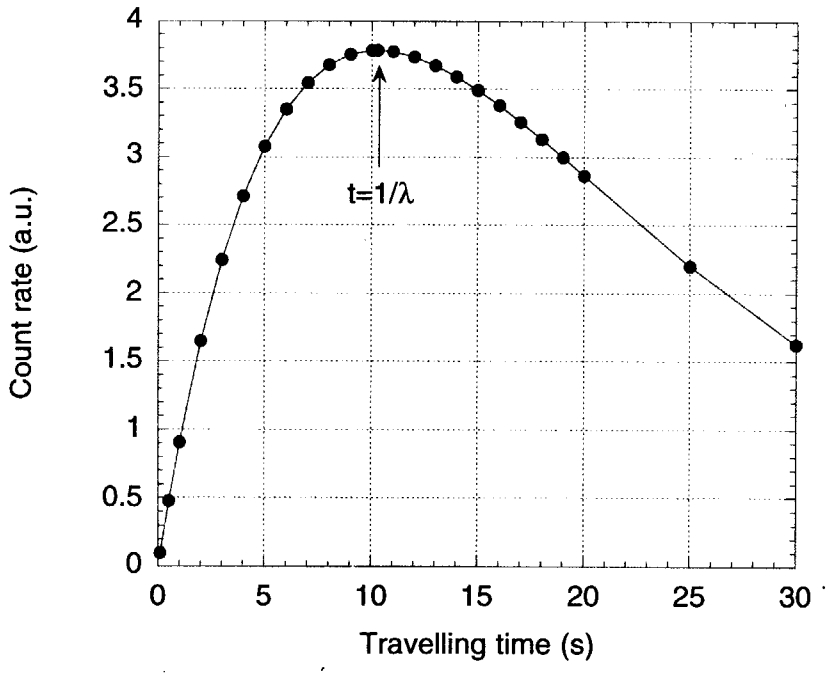

Figure 2.2-2 Gamma-ray counting rate as a function of travelling time.

2.3 Basic Theory of the Time Resolution

In the R&D task T499, we found that the time resolution of the neutron activation measurement with fluid flow is determined by dispersion in a turbulent flow. In the case of a cylindrical tube with diameter *d*, the Reynolds number is represented by

$$\mathrm{Re} = \frac{vd}{\nu} \tag{2.3-1}$$

where v is the flow velocity and ν is the kinetic viscosity of water. The range of the Reynolds number considered here is shown in Fig.2.3-1. In the range of Reynolds number larger than ~2000, the flow is turbulent. Therefore we discuss turbulent flow only.

The tracer particle, which is ^{16}N nuclei here, is generated at t = 0 and x =0 as shown in Fig.2.3-1. Even in a turbulent flow, the flow velocity has a distribution in the radial direction. However, the tracer density *C* will be homogeneous in the radial cross section after a mixing length defined by $L_{mix} = 1.5\ d\ Re^{1/5}$. We can consider the dispersion in the x direction only. The tracer density C is determined by the following equation;

$$\frac{\partial C}{\partial t} + v\frac{\partial C}{\partial x} = \kappa\frac{\partial^2 C}{\partial x^2} \tag{2.3-2}$$

This has the same form as the one-dimensional diffusion equation. Therefore, the solution is

$$C(x,t) = \frac{1}{(4\pi t\kappa)^{1/2}}\exp\left(-\frac{(x-vt)^2}{4\kappa t}\right) \tag{2.3-4}$$

This solution means that the tracer distribution at time *t* is a Gauss distribution with $\sigma^2 = 2\kappa t$. So the FWHM ΔW is

$$\Delta W = 2.35\sigma$$
$$= 2.35\ (2\kappa t)^{1/2} \tag{2.3-5}$$

In the case of a cylindrical tube with diameter *d*= *2a*, the dispersion coefficient κ is

$$\kappa = 10.1\, U_\tau\, a \tag{2.3-6}$$

where U_τ is a friction velocity and represented by

$$U_\tau = v\sqrt{\frac{f}{8}}$$
$$f = \frac{0.316}{Re^{1/4}} \tag{2.3-7}$$

for a smooth inner surface tube. Finally the time resolution of the measurement Δt is represented by,

$$\Delta t = \Delta W/v$$
$$= 4.71(aL_1)^{1/2}/(vRe^{1/16})$$

which is almost proportional to *1/v* or the travelling time *t*.

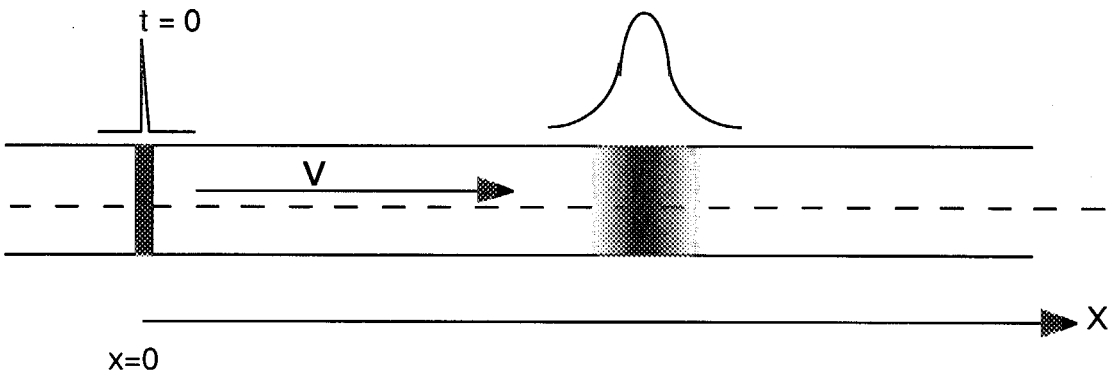

Figure 2.3-1 Model of time resolution calculation based on dispersion in a turbulent flow.

2.4 Gamma-ray Detector and Gamma-ray Counting Station

2.4.1 Selection of the gamma-ray detector

In the energy range higher than 5 MeV, gamma-rays are measured with electron and positron pair creation processes. The cross-section of the pair creation increases with the square of the charge number Z of the detector material. Therefore high Z materials are suitable for the detection of 6.13 and 7.12 MeV gamma-rays. We employed a BGO ($Bi_4Ge_3O_{12}$) scintillator, because the density of BGO, 7.13 g/cm^3, is twice of that of NaI scintillator which is the most conventional and popular gamma-ray detector. The size of the BGO scintillator is 12.5 cm (5 inch) in diameter by 12.5 cm (5 inch) long, which is the largest in the commercially available BGO scintillator.

The time constant of the scintillation light is 400 ns in the BGO scintillator. If we define the count rate limit by a 10 % dead time, the maximum count rate is 2.5×10^5 counts/s for the BGO scintillator, which is almost similar for other inorganic scintillators.

2.4.2 Gamma-ray counting station

The gamma-ray counting station has to be installed in the low-background region. The candidate of the location is a place in a pit away form the coolant water pipes for the blanket modules and the vacuum vessel, which are intense gamma-ray source by ^{16}N. We proposed a pair of the BGO scintillator detectors with different geometrical efficiencies in a gamma-ray counting station as shown in Fig.2.4-1. Detector #1 faces the water tube directly, and detector #2 has a collimator with an aperture size of 50 mm × 50 mm × 200 mm.

2.4.3 Pulse height distribution and detection efficiency

The expected pulse height distribution for unit activity of ^{16}N was calculated by MCNP-4b code based on the model of the gamma-ray counting station shown in Fig. 2.4-1. Figure 2.4-2 shows the calculated pulse height distributions for detectors #1 and #2, where the branching ratio of the 6.13 and 7.12 MeV gamma-rays is taken into account. Full energy peaks of 6.13 and 7.12 MeV, a single photon escape peak, and the annihilation peak of 0.511 MeV are identified.

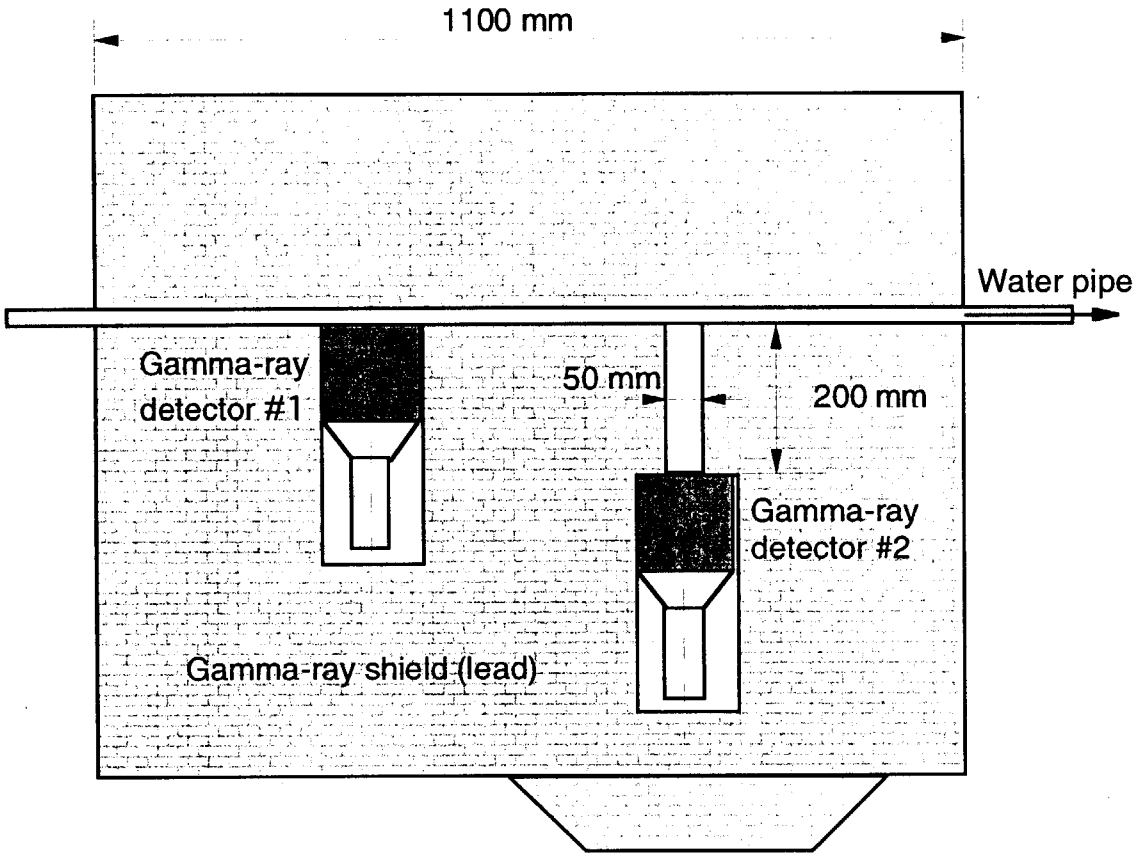

Figure 2.4-1 Concept of the gamma-ray counting station.

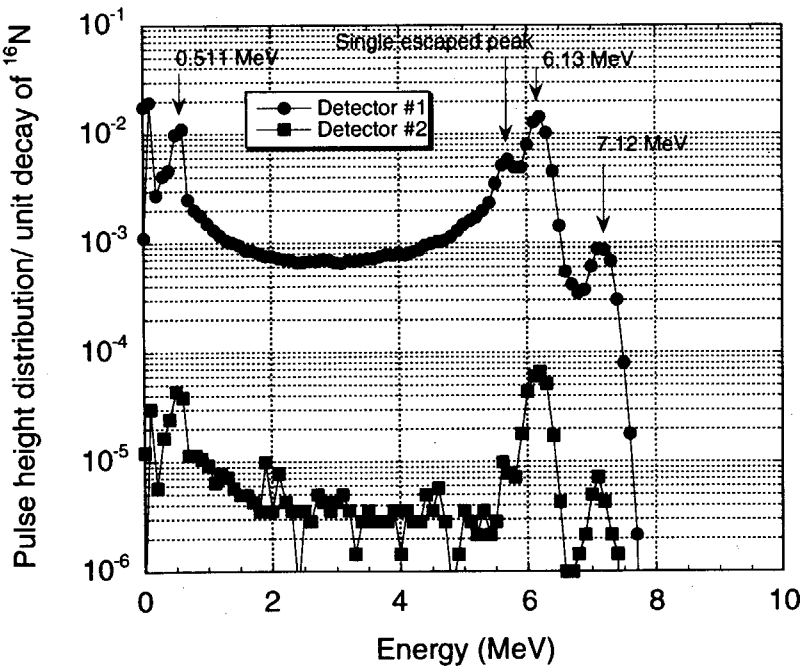

Figure 2.4-2 Calculated pulse height distributions for a unit activity of ^{16}N.

In this measurement, gamma-rays are counted by a scalar. The detection efficiency depends on the discrimination level (lower discrimination level) of the pulse height as shown in Fig. 2.4-3, where the intrinsic detection efficiency of the detector, the geometrical efficiency, and γ-ray emission probability were taken into account. Typical settings of the discrimination level are listed in Table 2.4-1. From the background rejection point of view, the window of the discrimination levels should be as narrow as the full energy peak width, but a much wider window width may be desired to get a sufficient count rate during the low fusion power operation.

Table 2.4-1 Typical settings of the discrimination levels and the detection efficiencies.

Case #	Lewer limit (MeV)	Upper limit (MeV)	Detection efficiency #1	Detection efficiency #2	
1	5.2	6.8	8.27 E-2	2.99 E-4	6.13 MeV peak
2	5.2	8.0	8.69 E-2	3.23 E-4	6.13+7.12 MeV peaks
3	0.8	8.0	1.28 E-1	5.20 E-4	> 0.511 MeV peak
4	0.0	8.0	2.02 E-1	7.04 E-4	Total

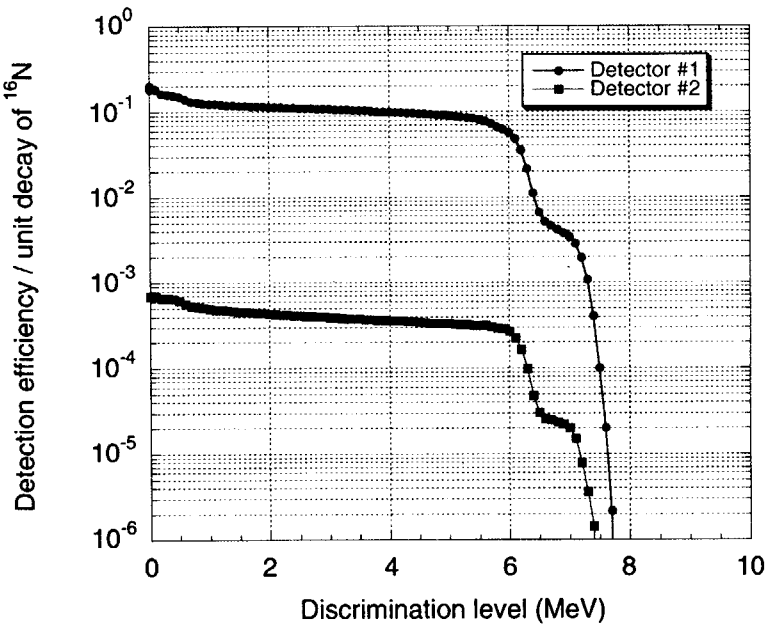

Figure 2.4-3 Detection efficiency as a function of the lower discrimination level. Here upper discrimination level is 8 MeV.

2.5 Installation Position of the Irradiation End

The $^{16}O(n,p)^{16}N$ reaction has a high threshold energy, so that the irradiation end should be as close to the plasma as possible. However, a bare water tube directly facing to the plasma is very dangerous, because the plasma could damage on the water pipe and cause a water leak inside the vacuum vessel. Here we proposed the irradiation end to be installed in the filler blanket module as shown in Fig.2.5-1. The water pipe is inserted into the filler module passing through the vacuum vessel and simply returns out from the filler module.

For the convenience of piping, filler modules near the horizontal port are a suitable for the installation position of the irradiation end.

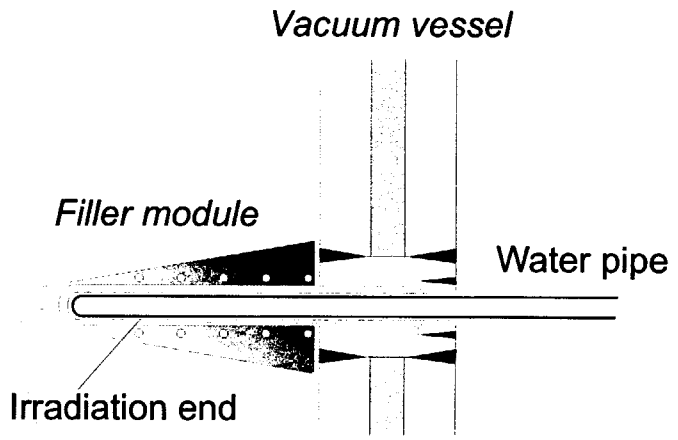

Figure 2.5-1 Concept of the irradiation end to be installed in the filler module.

2.6 Neutronics Calculation

2.6.1 Neutronics calculation model

We evaluated the reaction rate of the $^{16}O(n,p)^{16}N$ reaction in the irradiation end to a neutron Monte Carlo calculation using MCNP version 4b code[11]. Full sectors of the first wall, shielding blanket, some filler modules and the vacuum vessel are modeled. The divertor cassettes, ports and coils are not included. Toroidal gaps of the filler modules are modeled. However, poloidal gaps between adjacent blankets are not modeled. The calculation model around the irradiation end is shown in Fig 2.6-1. We use the neutron cross-section set based on JENDL 3.2[12].

The neutron source is a toroidally symmetric source with 14 MeV monoenergetic energy. The source has a poloidal distribution as follows;

$$s = \left[1 - \left\{\frac{\left(R - R_0 + \delta a - f(z)\right)^2}{a^2} + \frac{\left(z - Z_0\right)^2}{a^2 k^2}\right\}\right]^m$$

$$f(z) = \delta a \left[1 - \frac{\left(z - Z_0\right)^2}{a^2 k^2}\right]^n \qquad (2.6\text{-}1)$$

Where R_P is the major radius, a_P is the minor radius, Z_P is the vertical shift of the plasma center, κ is the ellipticity, δ is the triangularity and m is the power of the parabolic profile. Parameter n determines the triangular shape of the plasma. The angular emission is isotropic. The reference parameters are R_P = 6.2 m, a_P = 2.0 m, Z_P = 0.53 m, κ = 1.7, m = 0.8 and n = 0.5. This formula can represent the neutron source profile of ITER-FEAT. In this case, the neutron source peaking factor is represented by

$$\frac{S_n(0)}{\langle S_n \rangle} = m + 1 \qquad (2.6\text{-}2)$$

Where $S_n(o)$ and $<S_n>$ are the central and volume averaged neutron emissivity, respectively.

Energy groups in the MCNP calculation are shown in Table 2.6-1. The lowest energy is 8 MeV in the calculation, because the $^{16}O(n,p)^{16}N$ reaction has a threshold energy at 10.24 MeV.

Table 2.6-1 Energy group in the MCNP calculation.

Number	Upper Energy (MeV)	Lower Energy (MeV)	Lethergy width
1	9.3140E+00	8.2610E+00	1.1997E-01
2	1.0500E+01	9.3140E+00	1.1986E-01
3	1.1478E+01	1.0500E+01	8.9057E-02
4	1.2549E+01	1.1478E+01	8.9209E-02
5	1.3720E+01	1.2549E+01	8.9214E-02
6	1.5000E+01	1.3720E+01	8.9196E-02

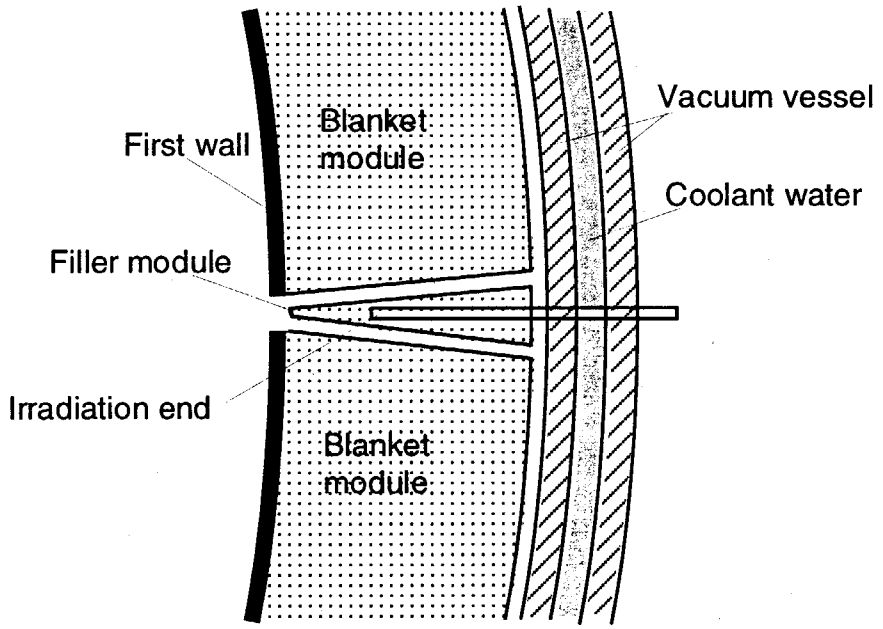

Figure 2.6-1 Calculation model around the irradiation end.

2.6.2 Neutron spectra and reaction rate in the irradiation region.

Calculated neutron spectra in the irradiation region are shown in Figure 2.6-2. In this calculation, the location of the irradiation end is assumed to be R=8.716 m and Z= +0.742 (from the center of the vacuum vessel).

The reaction rate distribution of $^{16}O(n,p)^{16}N$ along the water transfer tube is shown in Figures 2.6-3 and 2.6-4 (log plot). The FWHM of the reaction rate distribution is only 15 cm. If the flow velocity is 10 m/s, the time spread due to the width of the reaction rate distribution is 15 ms, which is much smaller than turbulent dispersion effects during the travelling from the irradiation end to the counting station.

The reaction rate along the transfer tube integrated from the irradiation end is shown in Fig.2.6-5. The activation in the filler module is 90 % of the total activation. The activation in the transfer tube farther than 40 cm from the irradiation end is negligible. The absolute value of the integrated reaction rate is 2.64×10^{10} cm/s for 1 g of water. The averaged reaction rate is 2.64×10^{9} /s, because effective length of the irradiation region is 10 cm.

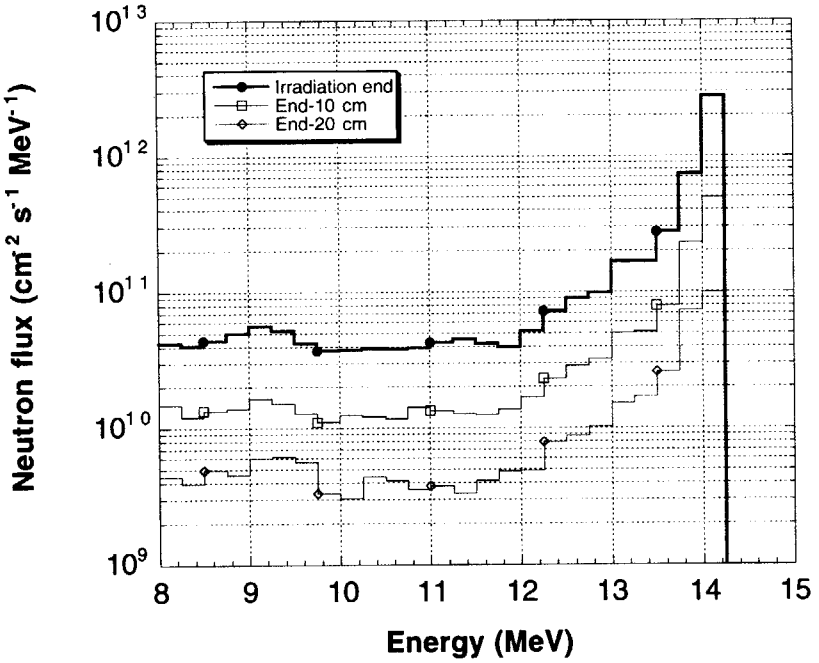

Figure 2.6-2 Calculated neutron spectra in the irradiation region.

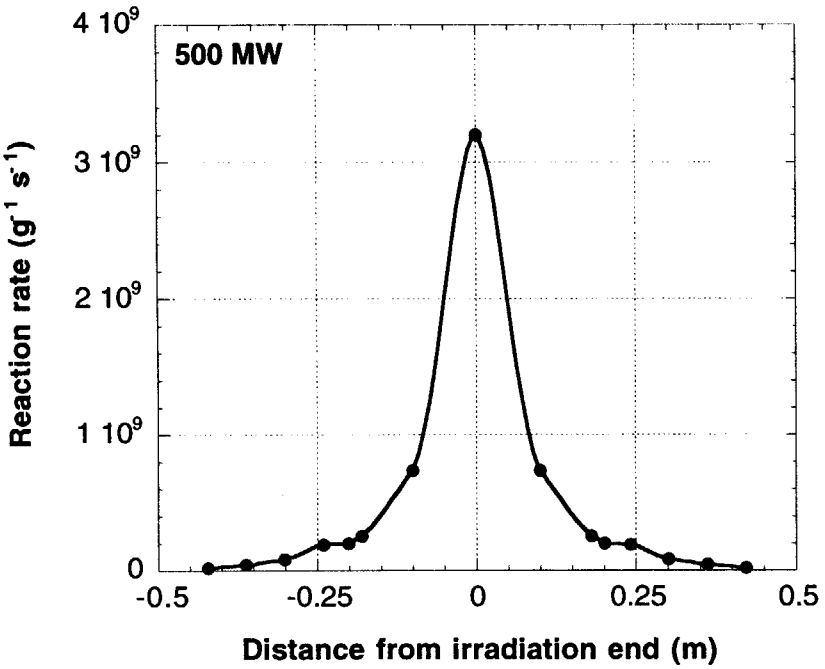

Figure 2.6-3 Reaction rate distribution of $^{16}O(n,p)^{16}N$ along the water tube (linear plot).

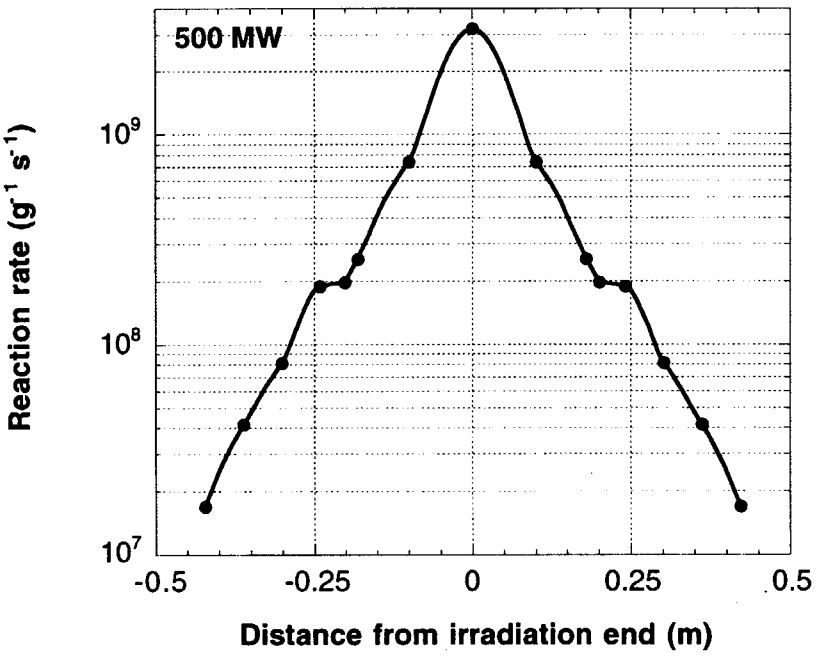

Figure 2.6-4. Reaction rate distribution of $^{16}O(n,p)^{16}N$ along the water tube (log plot).

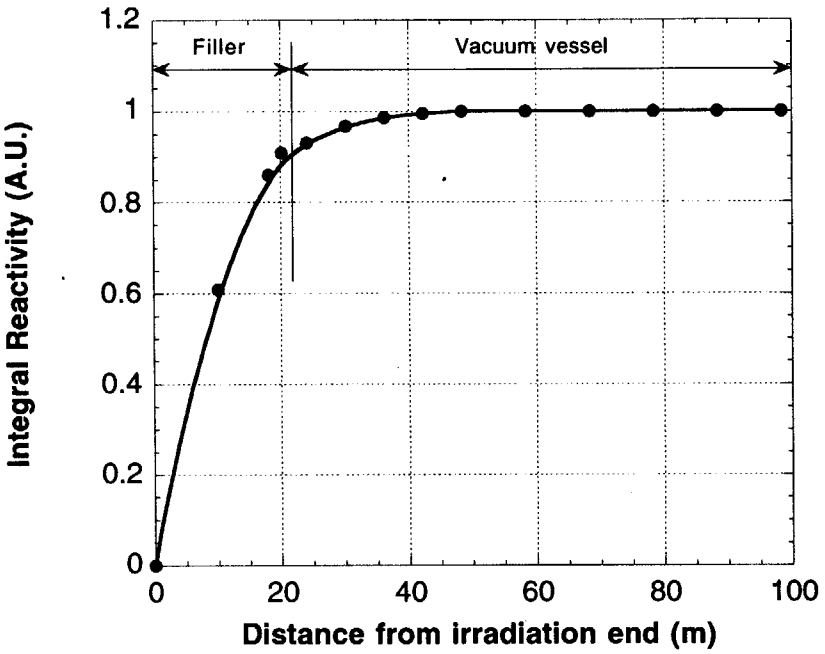

Figure 2.6-5 Integrated reaction rate along the water transfer tube.

2.6.3 Effect of the plasma position on the reaction rate

The reaction rate may be affected by the change of the plasma position, because the irradiation end is very close to the plasma. We evaluated the reaction rate of the $^{16}O(n,p)^{16}N$ reaction for the change of the plasma position using a source routine based on Eq.(2.6-1).

The dependence of the detection efficiencies for the horizontal plasma shift is shown in Fig.2.6-6. The reference plasma position is Rp =6.2 m and Zp = 0.53 m. The detection efficiencies are very weak functions of the horizontal plasma position. Difference of the reaction rate is not larger than 1%. Also the dependence of the relative reaction rate for the vertical plasma shift is shown in Fig. 2.6-7. The deviation is from -5% to +1%. Especially, the deviation is only ±1% in the range of Zp = 0.53 ±0.25 m.

Therefore, we can conclude that the reaction rate in the irradiation end is insensitive to the change of the plasma position.

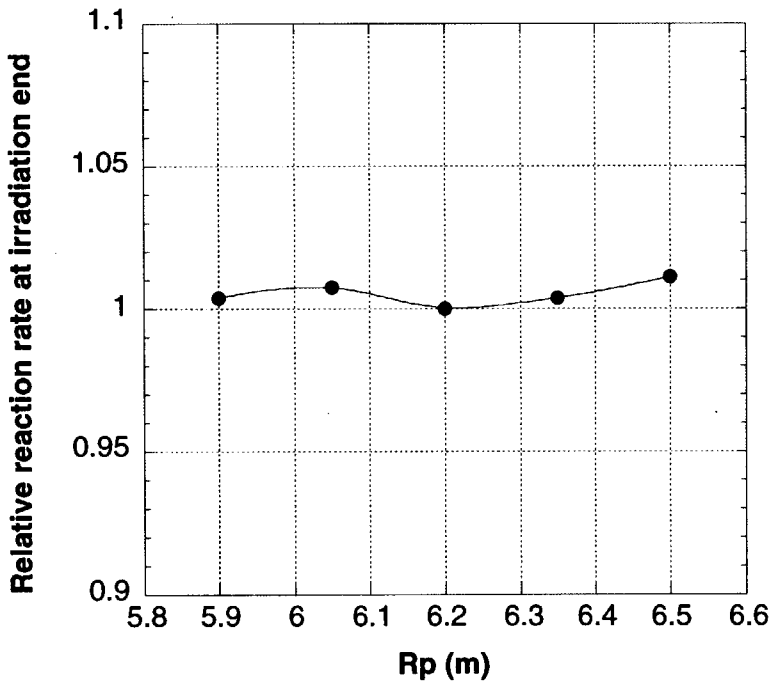

Figure 2.6-6 Dependence of the relative reaction rate in the irradiation end versus the horizontal plasma shift.

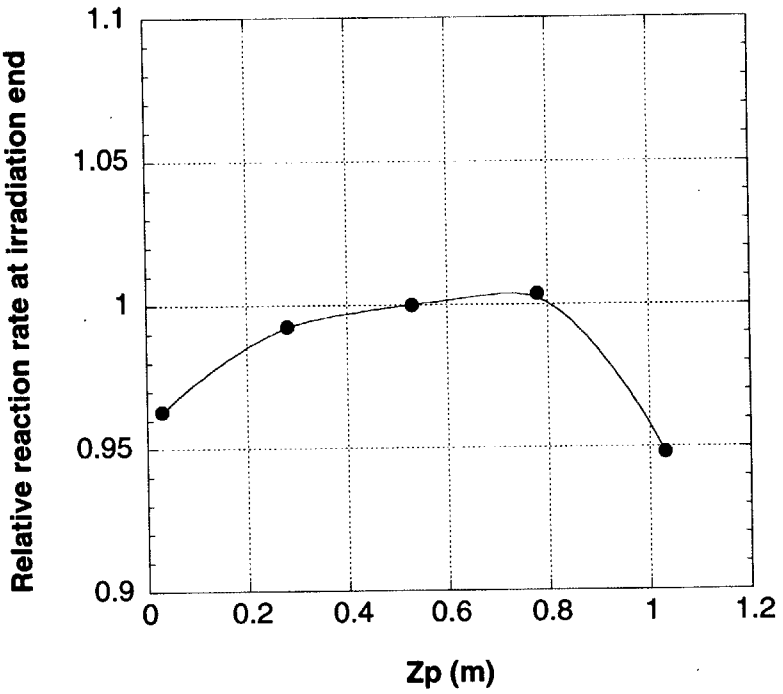

Figure 2.6-7 Dependence of the relative reaction rate in the irradiation end versus the vertical plasma shift.

2.7 Evaluation of the Time Resolution

Based on Eq (2.3-8), the time resolution is calculated as a function of the flow velocity with a water pipe diameter of 10, 20, and 30 mm as shown in Fig. 2.7-1. The length of the water pipe from the irradiation end to the gamma-ray counting station is assumed to be 20 m. The difference in the time resolution for the water pipe diameter is due to the diameter dependence of the Reynolds number shown in Eq. (2.3-1). In order to meet the time resolution requirement of 100 ms, we need a flow velocity of 7.3, 9.5, and 11.5 m/s for water pipe diameters of 10, 20, and 30 mm, respectively.

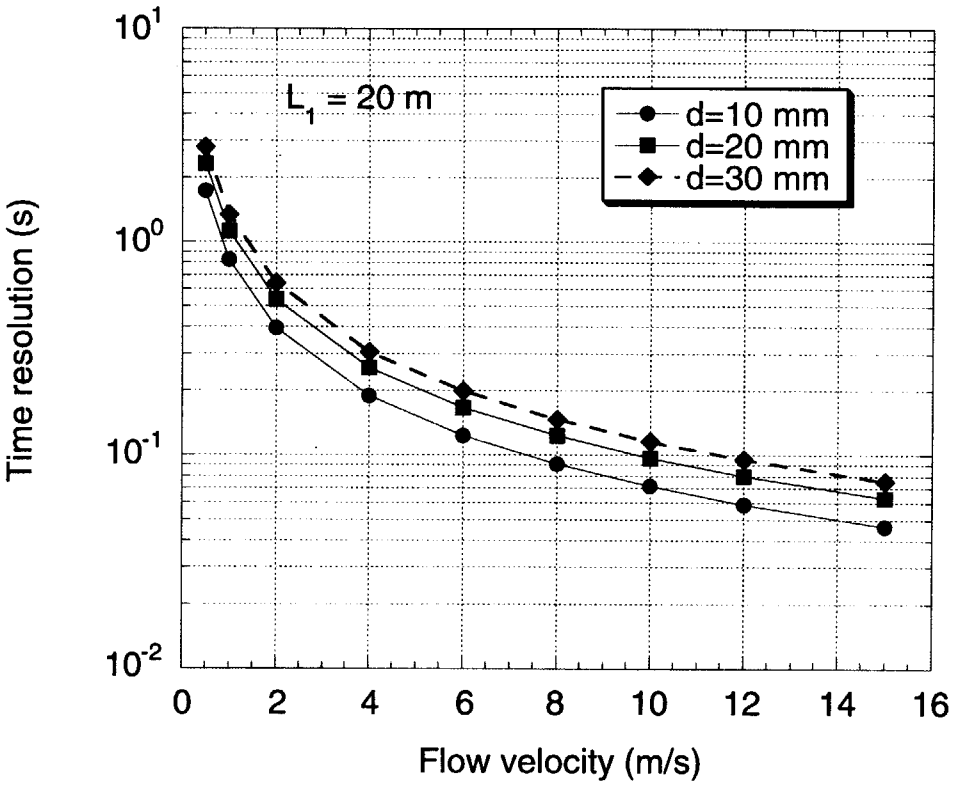

Figure 2.7-1 Calculated time resolution as a function of the flow velocity with a water pipe diameter of 10, 20, and 30 mm.

2.8 Evaluation of the Counting Rate and Dynamic Range

Figure 2.8-1 shows the count rates of the gamma-ray detectors. They are evaluated from Equations (2.2-3) and (2.2-4), where the detection efficiencies are case #1 in Table 2.4-1. For pulse counting, the maximum counting rate is limited up to 10^6 counts/s. Therefore, detector #1 will be saturated during 500 MW operation. In order to get a sufficient counting rate at lower fusion power, the diameter of the water pipe should be as large as possible. However, a larger diameter pipe needs a faster flow velocity to get a sufficient time resolution. The flow velocity of ~10 m/s is the maximum in the ordinal water loop. Here we employed the flow velocity of 10 m/s with a pipe diameter of 20 mm.

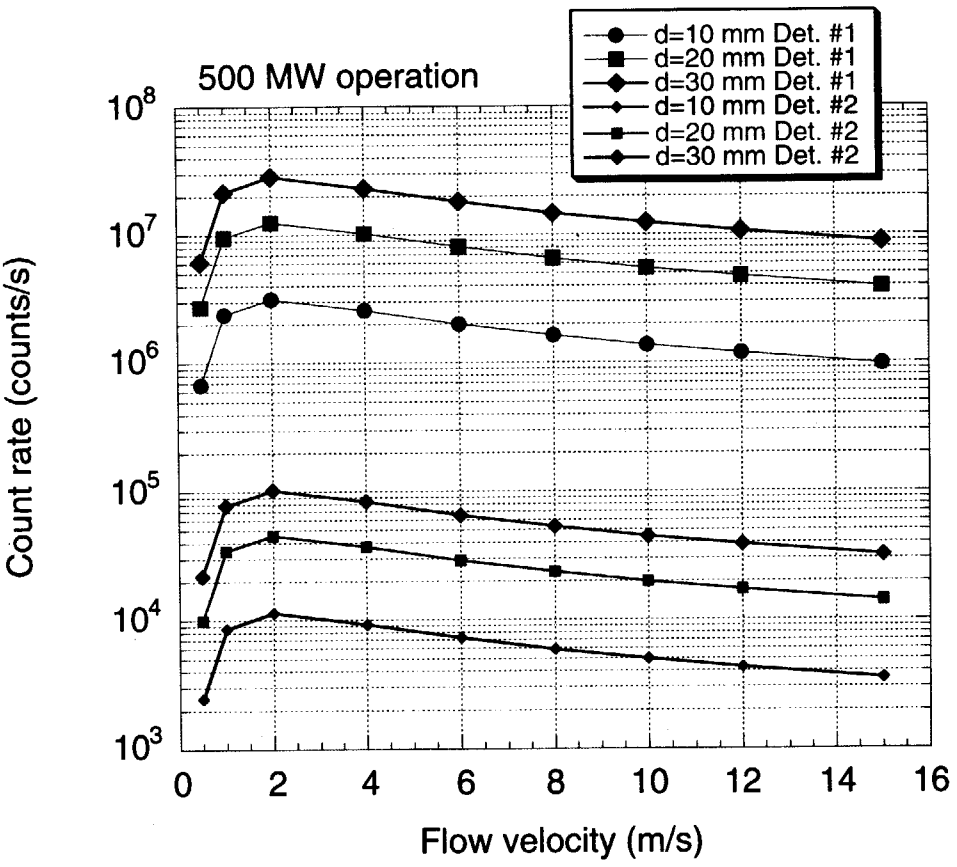

Figure 2.8-1 Calculated counting rate of the gamma-ray detectors as a function of the flow velocity with a water pipe diameter of 10, 20, and 30 mm.

If we define the lowest detection level as the statistical error of <10% for 100 ms counting duration, the counting rate must be between 10^3 and 10^6 counts/s. Figure 2.8-2 shows the range of the counting rate as a function of the fusion power. So we can measure the fusion power from 50 kW to 1000 MW of the ITER-FEAT operation, which corresponds to a neutron source strength of 10^{16}-10^{21} n/s, with the time resolution of 100 ms or less. If the time rsolution of 500 ms is allowed, we can extend the lower fusion power to 10 kW.

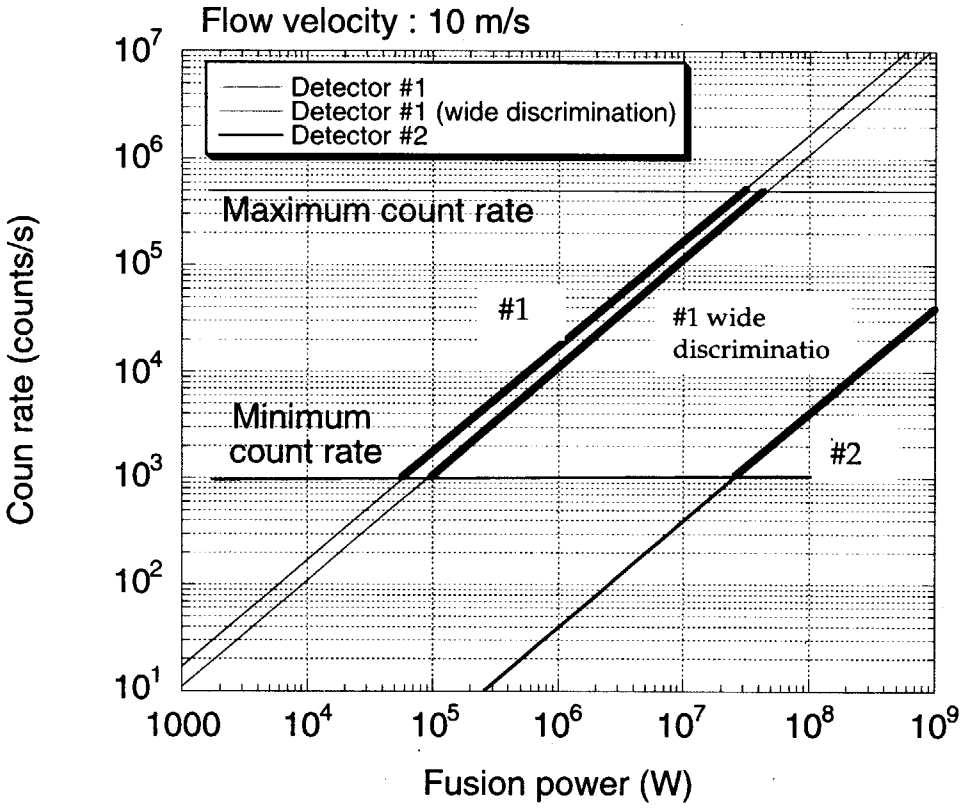

Figure 2.8-2 Calculated counting rate of the gamma-ray detectors as a function of the flow velocity with a water pipe diameter of 10, 20, and 30 mm.

2.9 Calibration

Absolute calibration of the source strength monitors is the most critical issue in the design of all neutron monitors. For the activation measurement, the relation ship of the reaction rate and the total neutron source strength can be calculated by MCNP code with a precise 3-D model of the tokamak, because the activation reaction with a high threshold energy such as 10 MeV is contributed by almost only the virgin D-T neutrons. Here we investigated the possibility of the direct calibration of the activation system with fluid flow.

We simulated *in-situ* calibration by MCNP calculation, where a point source of 14 MeV neutrons is moving on the plasma axis with R = 6.2 m and Z=0.53 m as shown in Figure 2.9-1. The irradiation end is in the filler module between blanket #13 and #14.

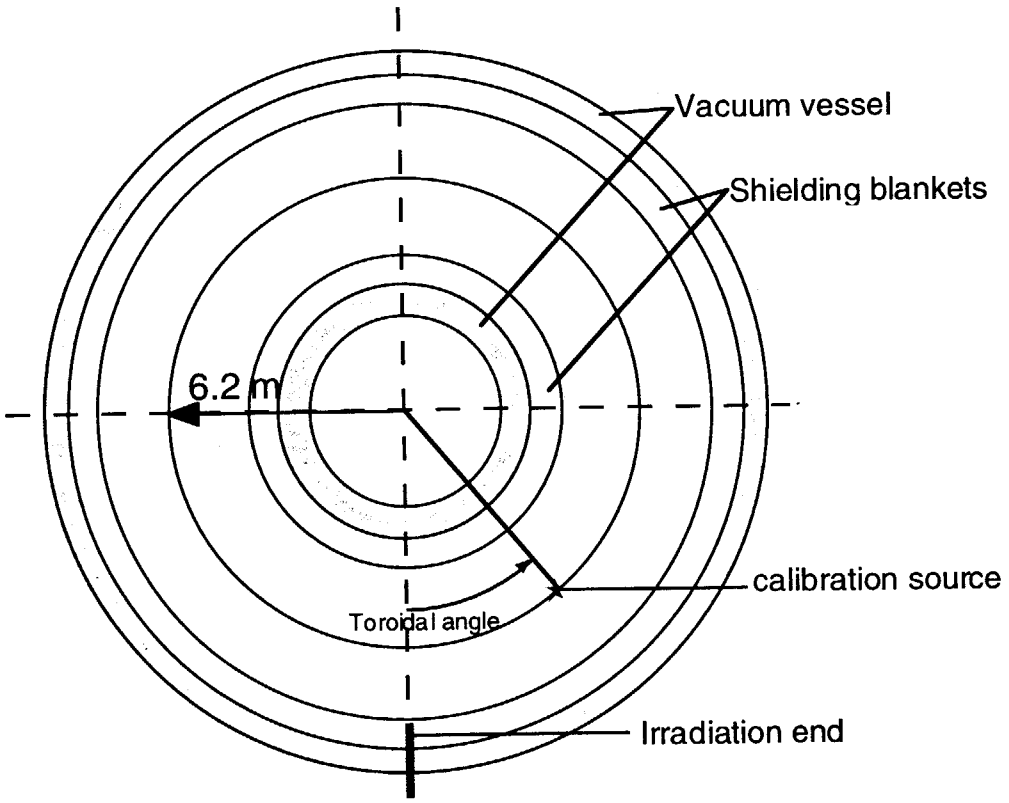

Figure 2.9-1 Calculation model of the *in-situ* calibration. A point source of 14 MeV neutrons is moving on the plasma axis with R = 6.2 m and Z=0.53 m.

Figure 2.9-2 shows the count rate of detector #1 for a point source of 10^{11} neutrons/s intensity on the plasma axis at R = 6.2 m plotted against the toroidal angle of the source. The activation reaction is contributed by neutrons in the range of the toroidal angle of ±30°, because the $^{16}O(n,p)^{16}N$ reaction has a high threshold energy.

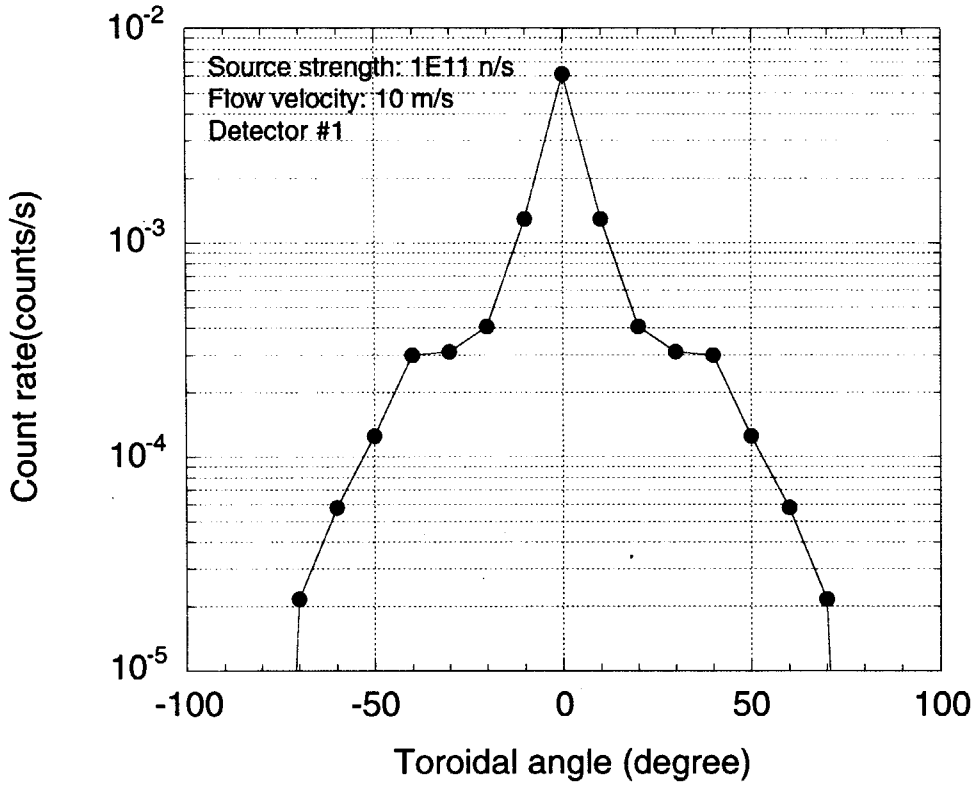

Figure 2.9-2 Calculation model of the *in-situ* calibration. A point source of 14 MeV neutrons is moving on the plasma axis with R = 6.2 m and Z=0.53 m.

A compact DT neutron generator with an emission rate of ~10^{11} neutrons/s has been developed by the Russian home team, which can be installed on the remote handling apparatus and can move inside the vacuum vessel. Even though we will use a DT neutron generator with an emission rate of 1×10^{11} neutrons/s, the count rate is expected to be only 6×10^{-3} counts/s at the toroidal angle of 0 degree. If we accumulate the counts for 1 day, expected counts is listed in Table 2.9-1. From the experience from Task T499, the background count rate due to cosmicrays is 10^{-3} - 10^{-4} counts/s. Therefore, the direct

calibration using the neutron generator is very difficult except the range of the toroidal angle of ±30 degree.

The neutron activation system with fluid flow should be calibrated with a combination of the MCNP calculation and the direct calibration using the neutron within ±30 degree. Otherwise, this system should be calibrated by a comparison with a neutron activation system using metal foils during real plasma operation. By those calibrations, the neutron activation system with fluid flow hopefully can meet the required 10% accuracy goals of the fusion power measurement for the ITER fusion power monitor.

Table 2.9-1 Expected counts for 1 day accumulation in the direct calibration using the neutron generator with a neutron intensity of 10^{11} n/s.

Toroidal angle (degree)	Count rate (counts/s)	Counts for 1 day (counts)	Statistical error	Relative error (%)
-70	2.16E-05	1.9	1.37	73.1
-60	5.77E-05	5.0	2.23	44.8
-50	1.25E-04	10.8	3.29	30.4
-40	3.00E-04	25.9	5.09	19.6
-30	3.10E-04	26.7	5.17	19.4
-20	4.07E-04	35.2	5.93	16.9
-10	1.29E-03	111.0	10.54	9.5
0	6.13E-03	530.0	23.02	4.3
10	1.29E-03	111.0	10.54	9.5
20	4.07E-04	35.2	5.93	16.9
30	3.10E-04	26.7	5.17	19.4
40	3.00E-04	25.9	5.09	19.6
50	1.25E-04	10.8	3.29	30.4
60	5.77E-05	5.0	2.23	44.8
70	2.16E-05	1.9	1.37	73.1

3. DETAILED SYSTEM DESCRIPTION

3.1 General Equipment Arrangement

The proposed arrangement of the fusion power monitor using water activation on ITER-FEAT is shown in Figures 3.1-1 - 3.1-2. One irradiation end will be installed in the filler module between the blanket #13 and #14 at port 17 passing through the horizontal port. Other irradiation ends in the filler module between the blanket #9 and #10 at the ports 1 and 5 passing through the upper ports.

The gamma-ray counting stations should be installed at well shielded location. So we propose the gamma-ray counting stations on the upstairs of the pit. In this case, the distance between the irradiation end and the counting station will be ~20 m. We should check the root of the cooling water pipes for the vacuum vessel and blanket, which will be background gamma-ray source in the energy range of 6-7 MeV. The electronics for the gamma-ray detectors will be installed in the pit near the gamma-ray counting stations.

The reservoir will be in the pit, which should be away from the gamma-ray counting stations.

3.2 Installation of the Irradiation End in the Filler Module

Figure 3.2-1 shows an isometric view of the irradiation end in the filler module. The guide tube will be welded into the vacuum vessel and the fuller module. The irradiation end will be inserted into the guide tube from the vacuum vessel.

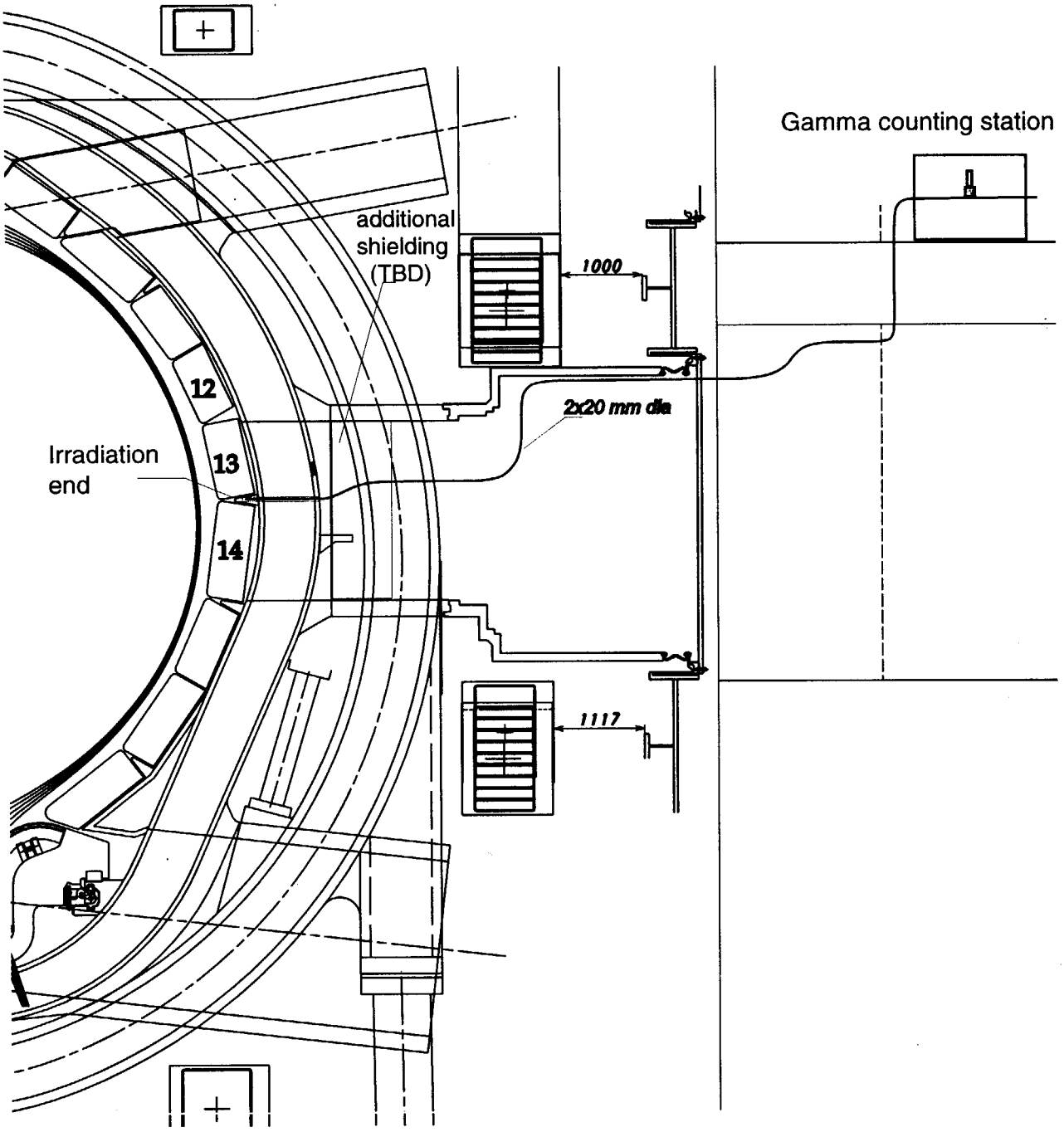

Figure 3.1-1 Arrangement of neutron activation system with fluid flow at the port 17.

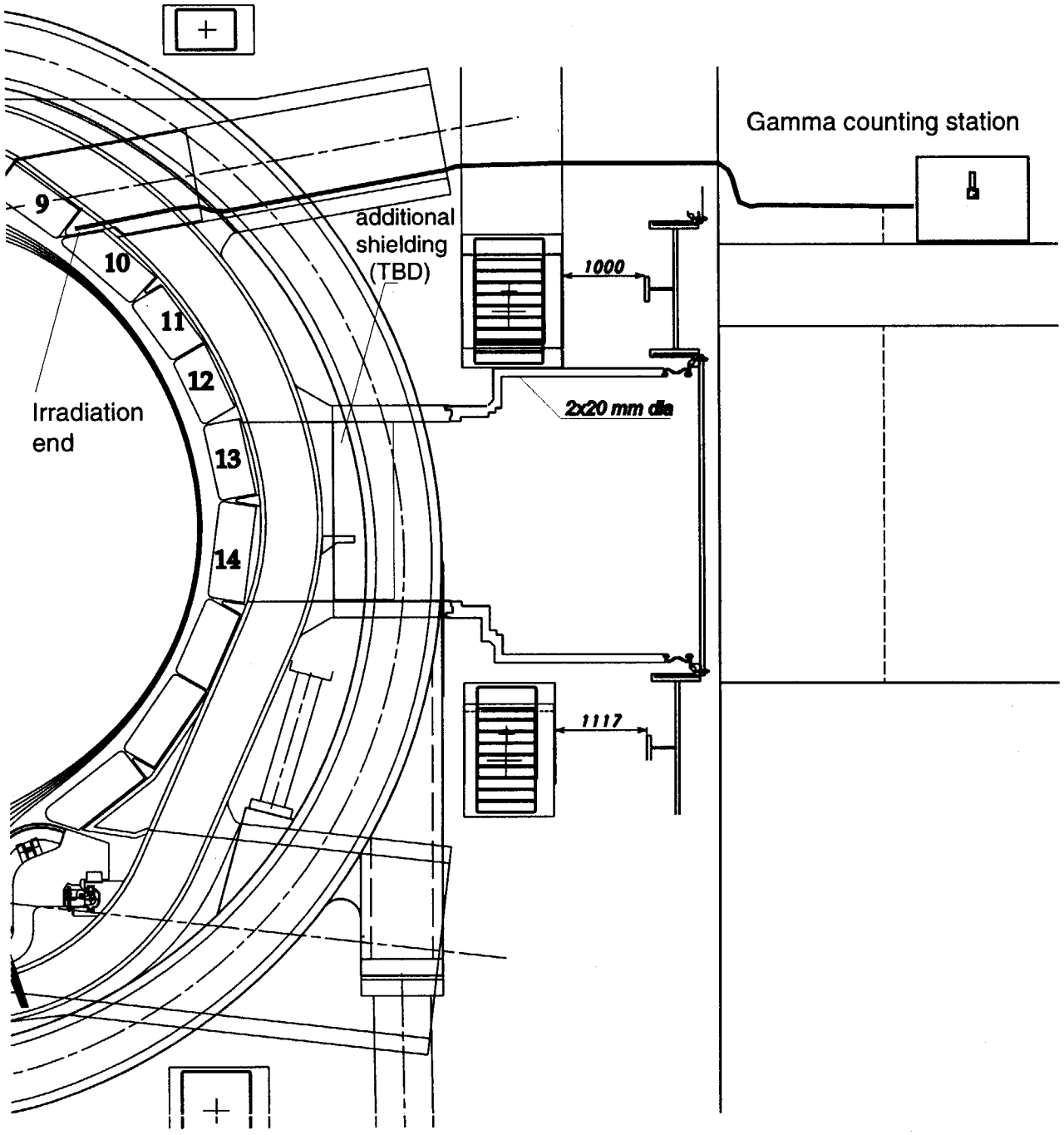

Figure 3.1-2 Arrangement of neutron activation system with fluid flow at the ports 1 and 5.

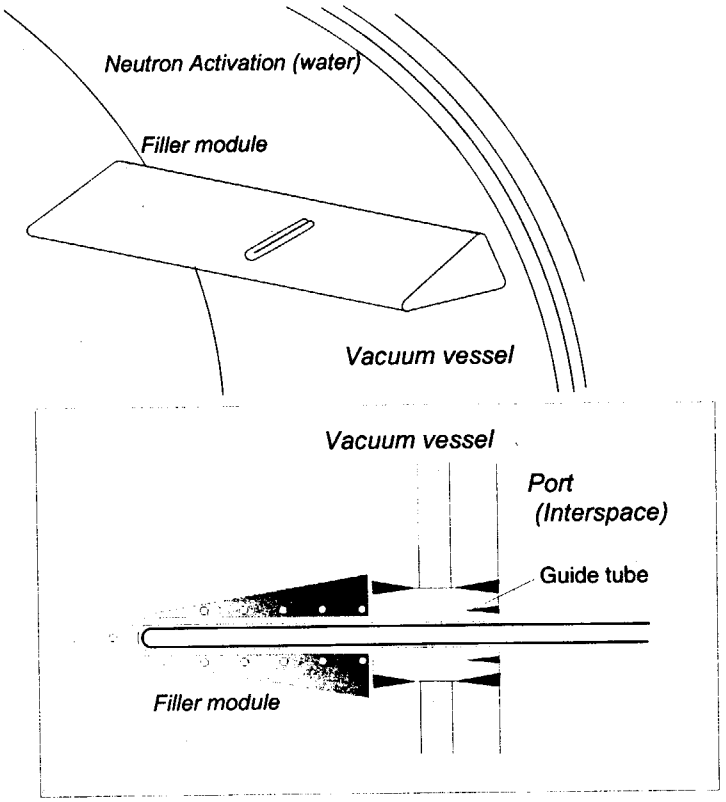

Figure 3.2-1. Installation of the irradiation end into the filler module and the vacuum vessel .

3.3 Water Loop

The water flow diagram of the neutron activation system with fluid flow is shown in Fig.3.3-1. Water will be pumped into the irradiation ends via a manifold from a reservoir. All valves will be operated by a workstation to control the water flow rate. The reservoir has baffles in order to decrease the radioactivity of the water.

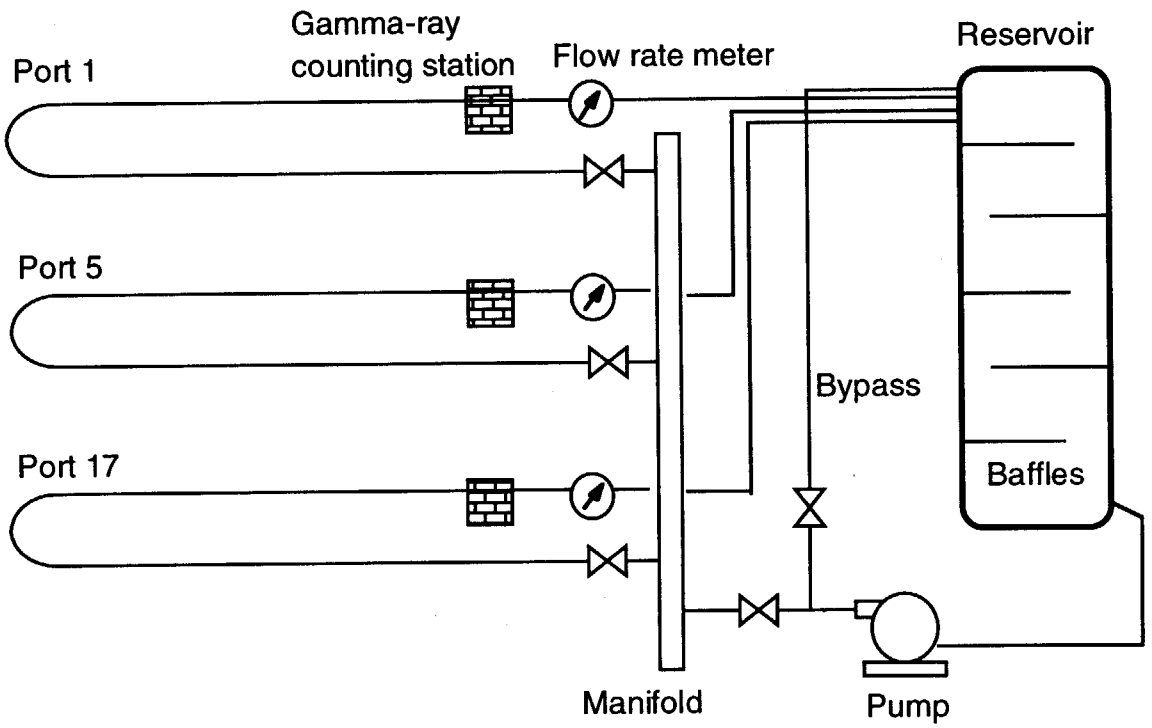

Figure 3.3-1 Water flow diagram of the neutron activation system with fluid flow.

3.4 Data Acquisition and Control

A block diagram of the electronics, the data acquisition equipment and the control is shown in Fig.3.4-1. Gamma-ray detectors will require high voltage power supplies, preamplifiers, linear amplifiers, pulse counting discriminators, and digital equipment, etc. The diagnostic data will be quired via a CAMAC or VME bus. The water flow velocity will be monitored and controlled with the workstation.

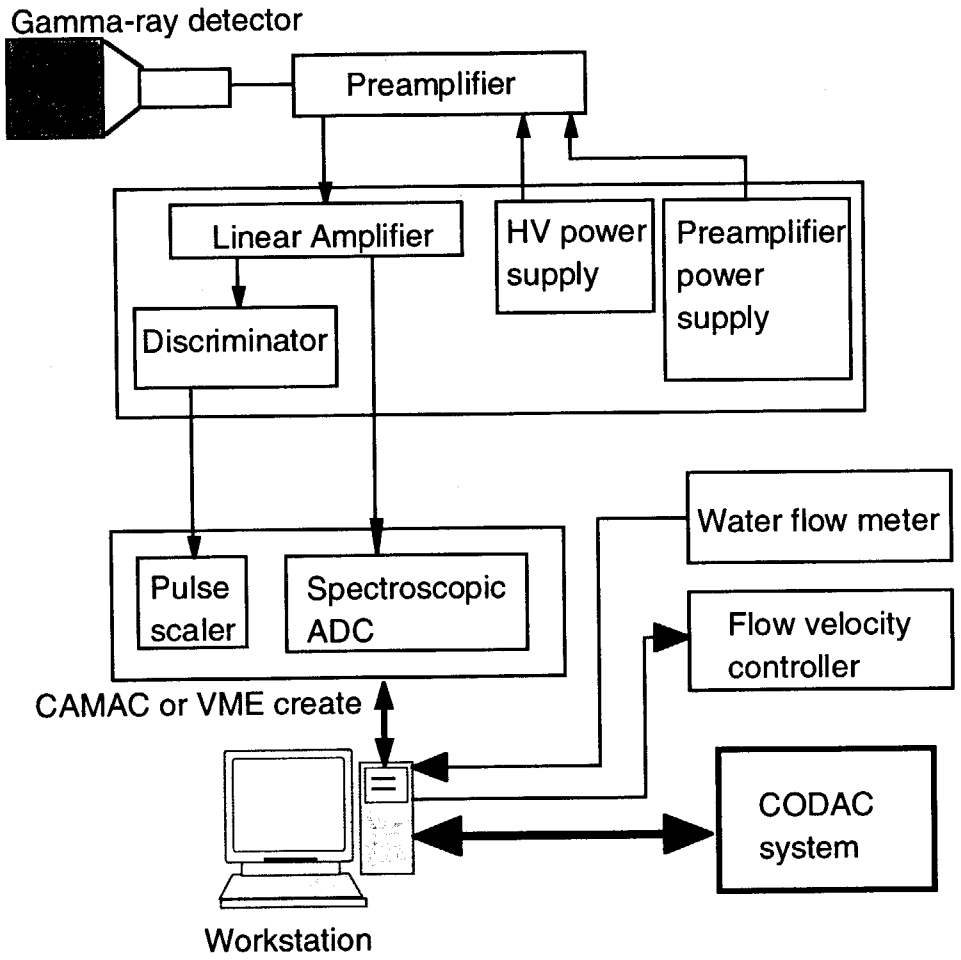

Figure 3.4-1 Block diagram of the electronics, the data acquisition and the control.

The policy of the data acquisition for all diagnostics has not been established. We estimated the data amount of the micro fission chamber system assuming that we will measure with constant sampling time for a whole discharge as shown in Table 3.4-1.

Table 3.4-1 Data amount of the micro fission chamber system.

	# Channel	Sampling time	Inductive operation 400 s	Hybrid operation 1000 s	Non-inductive operation 3000 s
Pulse counting	**4 ch × 2 detectors × 3 position**	**100 ms**	**192 kB**	**480 kB**	**1.44 MB**
Gamma-ray spectra	**1024 ch × 2 detectors × 3 position**	**100 ms**	**49.152 MB**	**122.88MB**	**368.64 MB**
Flow velocity	**× 3 position**	**100 ms**	**48 kB**	**120 kB**	**360 kB**
Total			**49.392 MB**	**123.48 MB**	**370.44 MB**

3.5 Calibration Hardware

As discussed in Section 2.9, in-situ calibration will be required to get sufficienct accuracy. An essential element of such calibrations is an intense, robust, yet compact DT neutron generator. The generator should produce 14 MeV neutrons at an average rate of ~10^{11} n/s, and be sufficiently compact and portable to allow operation inside the ITER vacuum vessel during initial system calibration and extended maintenance periods, using standard remote handling equipment, for in situ mapping of the reactivity for the point source. Of course this calibration hardware can be shared with the neutron flux monitor and other neutron diagnostics. So far, a neutron generator which has been developed by the Russian home team is one of the candidates [13].

3.6 Component List

List of Components is summarized in Table 3.6-1.

Table 3.6-1 List of equipment

Component	Quantity	Size (mm)	weight (kg)
Gamma-ray detector	6	ϕ125 × 400	10.0
Gamma-ray shield	3	900× 900× 1100	9800
Reservoir	1	ϕ800 × 1000	TBD
Water pipe	6	ϕ20 × 180000	TBD
Guide tube for filler and VV	3	ϕ24 × 10000	TBD
Water flow meter	3	TBD	TBD
Valve and controller	5	TBD	TBD
Pump	1	TBD	TBD
Preamplifier	6	100× 200 × 60	0.5
Preamplifier power supply	3	100× 200 × 100	1
Linear amplifier	6	TBD	0.5
HV power supply	6	TBD	2
Discriminator	3	TBD	0.5
CAMAC or VME create	2	800× 400× 700	20
NIM BIN create	3	800× 400× 500	10
ADC Module	6	TBD	TBD
Scalar Module	1	TBD	TBD
Workstation	1	TBD	TBD
Other Digital Modules	TBD	TBD	TBD
Local control cubicle	3	1000× 1000× 100 00	100
Neutron generator	1	TBD	TBD

4. OPERATION STATE DESCRIPTION

4.1 Commissioning State

All equipment should be installed in the commissioning stage of ITER. ITER has not commenced operation. All electronic equipment is accessible for testing.

4.2 Calibration State

The activation system with fluid flow is installed and operational. ITER has not commenced operation, and the vacuum vessel is open for in-vessel activities. The neutron generator and transport apparatus are temporarily installed inside the ITER vacuum vessel before initial pump-down. Personnel access is excluded in all areas affected by the operation of the neutron generator.

4.3 Experimental Operations State

All equipment is operational. ITER will be in operation. Personnel access is excluded, according to project safety requirements.

4.4 Maintenance State

ITER is not in operation. Access to equipment for maintenance activities is determined according to project safety requirements. Basically equipment inside the biological shield is maintenance free.

5. CRITICAL DESIGN AREAS AND R&D ITEMS

5.1 Critical Design Areas

- Arrangement of the reservoir and the pump in the diagnostics hall.
- Arrangement of the gamma-ray counting station in the pit.
- Evaluation of the background gamma-rays from other water piles for the blanket modules and the vacuum vessel..
- Evaluation of the tritium production in the closed water loop and its removal.
- Evaluation of the nuclear heating of the water and its cooling.
- Evaluation of the electro-magnetic force on the irradiation ends during disruptions.

5.2 Necessary R&D Items

Major R&D items have been done in the R&D Task T499. Residual R&D items are as follows;

- Effect of the temperature gradient along the water pipe from the irradiation end to the gamma-ray counting station.
- Test of the electro-magnetic force on the irradiation ends simulating disruptions.

6. CONCLUSION

We designed a neutron activation system with fluid flow based on the $^{16}O(n,p)^{16}N$ reaction for the accurate fusion power monitor with reasonable temporal resolution for ITER. Irradiation ends will be installed in the filler module between the blanket modules at the horizontal port and the upper ports. The gamma-ray counting stations will be installed on the upstairs of the pit. The distance between the irradiation end and the counting station is ~20 m.

We evaluated the performance of the neutron activation system with fluid flow based on the results of the R&D task T499. This system can measure the fusion power from 50 kW to 1000 MW of the ITER-FEAT operation, which corresponds to the neutron source strength of 10^{16}-10^{21} n/s, with a time resolution of 100 ms or less. We found by a neutron Monte Carlo calculation using MCNP version 4b code that the reaction rate in the irradiation end is relatively insensitive to the change of the plasma position.

This system will be calibrated with a combination of MCNP calculation and direct calibration using the neutron within ±30 degree, which will result in an accuracy of 10%. The neutron activation system with fluid flow can meet the required 10% accuracy for a fusion power monitor. However, this system could not be used for a real time feedback control due to the time delay of ~1 sec. The neutron activation system with fluid flow is useful for fusion power monitor with a moderate time resolution.

Acknowledgment

The authors would like to appreciate Mr. H. Kawasaki and Mr. M. Wada for his support on the neutronics calculations. We appreciate Dr. S. Yamamoto of ITER-JCT for his support on this work. The authors acknowledge the JMTR group for this irradiation test. This report has been prepared as an account of work assigned to the Japanese Home Team under Task Agreement number G 55 TD 02 95-11-24 FJ within the Agreement among the European Atomic Energy Community, the Government of Japan, the Government of the Russian Federation, and the Government of the United States of America on Cooperation in the Engineering Design Activities for the International Thermonuclear Experimental Reactor ("ITER EDA Agreement") under the auspices of the International Atomic Energy Agency (IAEA).

REFERENCES

[1] Firestone R. B. and Shirley V. S. (Eds.): "Table of Isotopes, Eighth Edition", John Wiley and Sons, Inc., New York, (1996).

[2] T. Nakagawa, K. Shibata, S. Chiba, et al., Japanese evaluated nuclear data library version 3 revision-2: JENDL-3.2, J. Nucl. Sci. Technol. 32, 1259(1995).

[3] Smith D. L., Gomes I. C., Ikeda Y., Uno Y., Maekawa F., Ward R. C. and Filatenkov A. A.: "Water Activation in a Fusion Environment", Fusion Technology, 30, 1049 (1996).

[4] ITER Documentation series No. 33, ITER DIAGNOSTICS, International Atomic Energy Agency, Vienna, p.116 (1991)

[5] Smith D. L., Ikeda Y., Uno Y. and Maekawa F.: "A New Method for Fast Neutron Dosimetry with a Circulating Liquid", Proc. of the 9th International Symposium on Reactor Dosimetry, Prague, Czech Republic, pp. 138-145 (1996).

[6] Ikeda Y., Uno Y., Maekawa F., Smith D. L., Gomes I. C., Ward R. C. and Filatenkov A. A.: "An Investigation of the Activation of Water by D-T Fusion Neutrons and Some Implications for Fusion Reactor Technology", Fusion Engineering and Design, 37, 107 (1997).

[7] C. Barnes, M. Loughlin, L.C. Johnson, K. Ebisawa, and T. Nishitani, "Neutron Activation for ITER", Rev. Sci. Instrum. 68, 577 (1997).

[8] Nakamura T., Maekawa H., Ikeda Y. and Oyama Y.:, "A DT Neutron Source for Fusion Neutronics Experiments at the JAERI", Proc. Int. Ion Eng. Congress – ISIAT '83 & IAPT '83, Kyoto, Japan, Vol. 1 pp. 567-570 (1983).

[9] J. Kaneko, Y. Uno, T. Nishitani, F. Maekawa, T. Tanaka, Y. Shibata, Y. Ikeda and H. Takeuchi, "Technal Feasibility Study on a Fusion Power Monitor Based on Activation of Water Flow", Rev. Sci. Instrum., 72, 809 (2001).

[10] V. Khripunov, private communication.

[11] J.F. Briesmeister (Ed.), MCNP - a general Monte Carlo n-particle transport code, version 4B, LA-12625-M, Los Alamos National Laboratory (1997).

[12] T. Nakagaea, K. Shibata, S. Chiba, et al., "Japanese evaluated nuclear data library version 3 reversion-2: JENDl-3.2", J. Nucl. Sci. Technol., 32, 1259 (1995).

[13] Yu.A. Kaschuck, D.V. Portnov, A.V. Krasilnokov, et al., "Compact Neutron Generator for Diagnostic Applications", Rev. Sci. Instrum. 70, 1104 (1999).

国際単位系 (SI) と換算表

表 1　SI 基本単位および補助単位

量	名称	記号
長さ	メートル	m
質量	キログラム	kg
時間	秒	s
電流	アンペア	A
熱力学温度	ケルビン	K
物質量	モル	mol
光度	カンデラ	cd
平面角	ラジアン	rad
立体角	ステラジアン	sr

表 2　SI と併用される単位

名称	記号
分，時，日	min，h，d
度，分，秒	°，′，″
リットル	l，L
トン	t
電子ボルト	eV
原子質量単位	u

1 eV = 1.60218 × 10^{-19} J

1 u = 1.66054 × 10^{-27} kg

表 5　SI 接頭語

倍数	接頭語	記号
10^{18}	エクサ	E
10^{15}	ペタ	P
10^{12}	テラ	T
10^{9}	ギガ	G
10^{6}	メガ	M
10^{3}	キロ	k
10^{2}	ヘクト	h
10^{1}	デカ	da
10^{-1}	デシ	d
10^{-2}	センチ	c
10^{-3}	ミリ	m
10^{-6}	マイクロ	μ
10^{-9}	ナノ	n
10^{-12}	ピコ	p
10^{-15}	フェムト	f
10^{-18}	アト	a

表 3　固有の名称をもつ SI 組立単位

量	名称	記号	他の SI 単位による表現
周波数	ヘルツ	Hz	s^{-1}
力	ニュートン	N	m·kg/s^2
圧力，応力	パスカル	Pa	N/m^2
エネルギー，仕事，熱量	ジュール	J	N·m
工率，放射束	ワット	W	J/s
電気量，電荷	クーロン	C	A·s
電位，電圧，起電力	ボルト	V	W/A
静電容量	ファラド	F	C/V
電気抵抗	オーム	Ω	V/A
コンダクタンス	ジーメンス	S	A/V
磁束	ウェーバ	Wb	V·s
磁束密度	テスラ	T	Wb/m^2
インダクタンス	ヘンリー	H	Wb/A
セルシウス温度	セルシウス度	℃	
光束	ルーメン	lm	cd·sr
照度	ルクス	lx	lm/m^2
放射能	ベクレル	Bq	s^{-1}
吸収線量	グレイ	Gy	J/kg
線量当量	シーベルト	Sv	J/kg

表 4　SI と共に暫定的に維持される単位

名称	記号
オングストローム	Å
バーン	b
バール	bar
ガル	Gal
キュリー	Ci
レントゲン	R
ラド	rad
レム	rem

1 Å = 0.1 nm = 10^{-10} m

1 b = 100 fm^2 = 10^{-28} m^2

1 bar = 0.1 MPa = 10^5 Pa

1 Gal = 1 cm/s^2 = 10^{-2} m/s^2

1 Ci = 3.7 × 10^{10} Bq

1 R = 2.58 × 10^{-4} C/kg

1 rad = 1 cGy = 10^{-2} Gy

1 rem = 1 cSv = 10^{-2} Sv

（注）

1. 表 1 − 5 は「国際単位系」第 5 版，国際度量衡局 1985 年刊行による。ただし，1 eV および 1 u の値は CODATA の 1986 年推奨値によった。
2. 表 4 には海里，ノット，アール，ヘクタールも含まれているが日常の単位なのでここでは省略した。
3. bar は，JIS では流体の圧力を表わす場合に限り表 2 のカテゴリーに分類されている。
4. EC 閣僚理事会指令では bar，barn および「血圧の単位」mmHg を表 2 のカテゴリーに入れている。

換　算　表

力	N(=10^5 dyn)	kgf	lbf
	1	0.101972	0.224809
	9.80665	1	2.20462
	4.44822	0.453592	1

粘　度　1 Pa·s(N·s/m^2) = 10 P(ポアズ)(g/(cm·s))

動粘度　1 m^2/s = 10^4 St(ストークス)(cm^2/s)

圧力	MPa(=10 bar)	kgf/cm^2	atm	mmHg(Torr)	lbf/in^2(psi)
	1	10.1972	9.86923	7.50062 × 10^3	145.038
	0.0980665	1	0.967841	735.559	14.2233
	0.101325	1.03323	1	760	14.6959
	1.33322 × 10^{-4}	1.35951 × 10^{-3}	1.31579 × 10^{-3}	1	1.93368 × 10^{-2}
	6.89476 × 10^{-3}	7.03070 × 10^{-2}	6.80460 × 10^{-2}	51.7149	1

エネルギー・仕事・熱量	J(=10^7 erg)	kgf·m	kW·h	cal(計量法)	Btu	ft·lbf	eV
	1	0.101972	2.77778 × 10^{-7}	0.238889	9.47813 × 10^{-4}	0.737562	6.24150 × 10^{18}
	9.80665	1	2.72407 × 10^{-6}	2.34270	9.29487 × 10^{-3}	7.23301	6.12082 × 10^{19}
	3.6 × 10^6	3.67098 × 10^5	1	8.59999 × 10^5	3412.13	2.65522 × 10^6	2.24694 × 10^{25}
	4.18605	0.426858	1.16279 × 10^{-6}	1	3.96759 × 10^{-3}	3.08747	2.61272 × 10^{19}
	1055.06	107.586	2.93072 × 10^{-4}	252.042	1	778.172	6.58515 × 10^{21}
	1.35582	0.138255	3.76616 × 10^{-7}	0.323890	1.28506 × 10^{-3}	1	8.46233 × 10^{18}
	1.60218 × 10^{-19}	1.63377 × 10^{-20}	4.45050 × 10^{-26}	3.82743 × 10^{-20}	1.51857 × 10^{-22}	1.18171 × 10^{-19}	1

1 cal = 4.18605 J (計量法)
= 4.184 J (熱化学)
= 4.1855 J (15 °C)
= 4.1868 J (国際蒸気表)

仕事率　1 PS (仏馬力)
= 75 kgf·m/s
= 735.499 W

放射能	Bq	Ci
	1	2.70270 × 10^{-11}
	3.7 × 10^{10}	1

吸収線量	Gy	rad
	1	100
	0.01	1

照射線量	C/kg	R
	1	3876
	2.58 × 10^{-4}	1

線量当量	Sv	rem
	1	100
	0.01	1

（86 年 12 月 26 日現在）

Design of Neutron Monitor using Flowing Water Activation for ITER